Parametric neutrino flavor conversions and Rabi oscillations

Lei Ma,* Shashank Shalgar,† and Huaiyu Duan‡
Department of Physics & Astronomy, University of New Mexico, Albuquerque, NM 87131, USA
(Dated: October 4, 2016)

We develop an interpretation of neutrino flavor conversions in fluctuating matter density based on Rabi oscillations. The interference as a result of multi-frequency matter density fluctuations is also explored and criteria of interference is proposed and verified numerically. Neutrino flavor conversion in matter with multiple-frequency fluctuations is expanded into superposition of Rabi oscillations to explain the relation between neutrino flavor conversion and Rabi oscillations precisely as well as providing more quantitative criteria on the interference between different frequencies of Rabi oscillations.

I. INTRODUCTION

In many astrophysical environments, such as core-collapse supernova, neutrinos propagate through dense fluctuating medium, which will interact with neutrinos and dramatically change the flavor oscillations of neutrinos. Meanwhile, neutrinos deposit energy in matter during the interaction, where the amount of energy deposited depends on the flavor of neutrinos. The significance of matter effect on neutrino flavor oscillations has been demonstrated in Mikheyev-Smirnov-Wolfenstein (MSW) effect [1–3], which is used to explain the deficit of electron flavor neutrino flux, thus solved the solar neutrino problem [4, 5]. Later developments on the theories about matter effect revealed the parametric resonance of neutrino flavor oscillations due to fluctuations in matter density [6, 7], which is the neutrino analog of transitions between energy levels as a result of external optical stimulation. Parametric resonance is different from the MSW effect since it involves the parameters of the matter density, which is usually the period of matter density fluctuations. Neutrinos passing through inside the Earth can experience parametric resonance [8, 9].

As one of the most intense neutrino sources, supernova neutrinos experience turbulent matter density as they propagate through out the explosion [10, 11], where the flavor conversion is modified by interaction with matter. Meanwhile with neutrinos depositing energy into the shock, neutrino flavor conversion is crucial to the shock evolution of supernova explosion. The turbulent matter density environment for neutrino flavor conversion has been researched [12–14]. Recently matter stimulated neutrino flavor conversion in varying matter density has been researched using Jacobi-Anger expansion by Kneller, et al. [15, 16]. They have shown that many stimulated neutrino flavor conversions can be explained by resonances of the system.

In this paper, we take a step further and interpret parametric resonance [6, 7] as well as other stimulated neutrino flavor conversions [15, 16], as superposition of Rabi oscillations. In Sec. II, we define the formalism of neutrino flavor conversions in matter used in this paper where the equation of motion and Hamiltonian for neutrino flavor conversion in matter are explicitly written. In Sec. III we discuss how neutrino flavor conversions are related to Rabi oscillations by neglecting less important terms and show that the system can be reduced to Rabi oscillations systems. Single frequency matter profile, castle wall matter profile are calculated and interpreted as Rabi oscillations. Interference effect between different frequencies are explained using two-frequency matter profile and three-frequency matter profile. In Sec. IV we discuss the technique of decomposing the neutrino flavor conversions into summation of Rabi oscillations, by applying a specific unitary transformation and the Jacobi-Anger expansion. In this section, we explain the reason why the approximations in Sec. III can be done.

II. BACKGROUND AND FORMALISM

We consider two-flavor oscillation scenario, in which neutrinos have energy E and mass-squared difference δm^2 between two mass states propagate through matter which is define by electron number density profile $n(r)$ along the path of neutrino propagation r. Three different bases are used in this work, i.e., flavor basis, in which the wave function describes the probability amplitude of different flavors, background matter basis, in which the wave function describe the probability amplitude of different mass states with the appearance of only background matter density, and Rabi basis which will be defined explicitly later. The dynamics of neutrino flavor conversion is determined by Schrödinger equation, in which the Hamiltonian in flavor basis is

$$H^{(\mathrm{f})} = \frac{1}{2}\begin{pmatrix} -\omega_{\mathrm{v}}\cos 2\theta_{\mathrm{v}} + \lambda(r) & \omega_{\mathrm{v}}\sin 2\theta_{\mathrm{v}} \\ \omega_{\mathrm{v}}\sin 2\theta_{\mathrm{v}} & \omega_{\mathrm{v}}\cos 2\theta_{\mathrm{v}} - \lambda(r) \end{pmatrix}, \quad (1)$$

where $\lambda(r) = \sqrt{2}G_{\mathrm{F}}n(r)$ is the potential of neutrino interaction with matter and G_{F} is the Fermi constant, θ_{v} is the vacuum mixing angle, $\omega_{\mathrm{v}} = \delta m^2/2E$ is the vacuum oscillation frequency. For the convenience of notation,

* leima@unm.edu
† shashankshalgar@unm.edu
‡ duan@unm.edu

we use Pauli matrices σ_i to denote the Hamiltonian, so that the Schrödinger equation becomes,

$$\mathrm{i}\frac{\mathrm{d}}{\mathrm{d}r}\Psi(r) = \frac{1}{2}\left((-\omega_\mathrm{v}\cos 2\theta_\mathrm{v} + \lambda(r))\sigma_3 + \omega_\mathrm{v}\sin 2\theta_\mathrm{v}\sigma_1\right)\Psi(r), \tag{2}$$

where $\Psi(r)$ is the wave function in flavor basis. For two flavor scenario, it is written as $\Psi(r) = (\psi_e, \psi_x)^\mathrm{T}$ where ψ_e and ψ_x are the amplitudes for electron flavor and the second flavor (μ flavor or τ flavor) respectively. The equation of motion in flavor basis governs the transitions between different flavors.

The potential $\lambda(r)$ for a general perturbation on top of a constant matter profile can be written as

$$\lambda(r) = \lambda_0 + \delta\lambda(r). \tag{3}$$

For better understanding of the transition between states as a consequence of the fluctuation of matter density, we use the background matter basis, in which the Hamiltonian is diagonalized in the absence of perturbation $\delta\lambda(r)$, so that the Hamiltonian reads

$$H^{(\mathrm{m})} = -\frac{\omega_m}{2}\sigma_3 + \frac{1}{2}\delta\lambda(r)\cos 2\theta_\mathrm{m}\sigma_3 - \frac{1}{2}\delta\lambda(r)\sin 2\theta_\mathrm{m}\sigma_1, \tag{4}$$

where θ_m is the mixing angle in a constant matter profile λ_0, which is calculated using relation

$$\tan 2\theta_\mathrm{m} = \sin 2\theta_\mathrm{v}/\left(\cos 2\theta_\mathrm{v} - \lambda_0/\omega_\mathrm{v}\right)$$

with ω_v denoting the vacuum oscillation frequency and θ_v denoting the vacuum mixing angle. The energy split is defined as

$$\omega_\mathrm{m} = \omega_\mathrm{v}\sqrt{(\lambda_0/\omega_\mathrm{v} - \cos(2\theta_\mathrm{v}))^2 + \sin^2(2\theta_\mathrm{v})}. \tag{5}$$

III. PARAMETRIC RESONANCE AND RABI OSCILLATION — A SIMPLIFIED MODEL

In this section we present a simple picture to explain neutrino parametric resonance in matter by utilizing the theory of Rabi oscillations which have been well studied in quantum optics [17]. In Appendix A, we derive the Rabi oscillation transition probabilities using neutrino flavor isospin method introduced in Ref. 18.

A. Single Frequency Matter Profile

The first example we examine is single frequency matter profile $\delta\lambda(r) = \lambda_1\sin(k_1 r)$. As will be proved later, the varying σ_3 term $\delta\lambda(r)\cos 2\theta_\mathrm{m}\sigma_3/2$ in Hamiltonian Eq. (4), which is the varying energy gap due to varying matter density fluctuations, has little effect on the transition probabilities when the system is close to resonance. With the varying σ_3 term removed, it indicates that this single frequency matter perturbation neutrino flavor conversion system is reduced to a Rabi oscillation system, with external driving field frequency k_1 and energy gap ω_m. By neglecting the off-resonance terms, the Hamiltonian can be simplified,

$$\begin{aligned} H^{(\mathrm{m})} &\to -\frac{\omega_\mathrm{m}}{2}\sigma_3 - \frac{1}{2}\lambda_1\sin 2\theta_\mathrm{m}\sin(k_1 r)\sigma_1 \\ &\to -\frac{\omega_\mathrm{m}}{2}\sigma_3 - \frac{1}{2}A_1\cos(k_1 r)\sigma_1 + \frac{1}{2}A_1\sin(k_1 r)\sigma_2, \end{aligned} \tag{6}$$

where

$$A_1 = \frac{\lambda_1\sin 2\theta_\mathrm{m}}{2i}. \tag{7}$$

The resonance condition is determined by matching the energy gap ω_m with external driving field frequency k_1, i.e., $\omega_\mathrm{m} \sim k_1$. As the system is approaching resonance condition, the transition probability is predicted well using Rabi formula. As defined in Appendix A, relative detuning $Q = |k_1 - \omega_\mathrm{m}|/|A_1|$ measures how off-resonance a system is. $Q \to 0$ indicates the system is very close to resonance, while $Q \to \infty$ indicates the system is far away from resonance.

To show that this conjecture of simplifying neutrino flavor conversions to Rabi oscillations is correct, we calculate transition probabilities of the neutrinos described by Eq. (4), and Rabi formula Eq. (A10) from the Rabi oscillations described by Eq. (A1). In FIG. 1, black dots show the transition probability of neutrino flavor conversions in matter, while solid line stands for the result predicted using Rabi formula. The corresponding relative detuning is $Q = 0$ as we have chosen $k_1 = \omega_\mathrm{m}$, which sets the system on exact resonance and explains the agreement between Rabi formula and the numerical calculation.

For a single-frequency perturbation in matter profile $\lambda(r) = \lambda_1 + \lambda_1\sin(k_1 r)$, P. Krastev and A. Smirnov concluded that the parametric resonance condition is $\omega_\mathrm{m} \sim nk_1$, if instantaneous $\omega_{\mathrm{m,inst}}(r)$ associated with the matter profile at distance r varies slowly [6]. This condition is exactly the Rabi resonance condition when $n = 1$, as such condition matches the driving field frequency to the energy split. All the $n > 1$ cases in their condition corresponds to the higher modes derived in Sec. IV.

B. Castle Wall Matter Profile

The approach applied to single frequency matter profile also helps with the understanding of multiple frequency matter profile. Since any matter profile can be

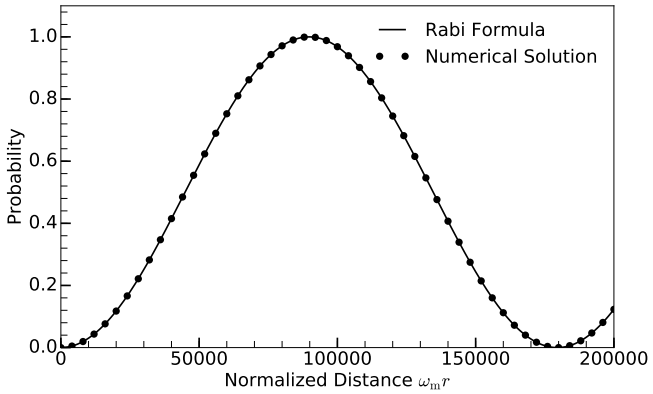

FIG. 1: Single frequency matter profile and Rabi oscillation. Black dots are the transition probabilities between two background mass eigenstates for the neutrinos with matter perturbation $A_1 \sin(k_1 r)$. During the calculation, λ_0 is set to 0.5 of the MSW resonance potential $\lambda_{\rm MSW} = \omega_{\rm v} \cos 2\theta_{\rm v}$ and mixing angle is chosen so that $\sin^2(2\theta_{\rm v}) = 0.093$. The solid line is the probabilities predicted using Rabi formula.

Fourier decomposed into superposition of many single frequency matter profile, we show an example of another well studied matter profile which is the periodic castle wall matter profile. The potential shown in Fig. 2 is defined as,

$$\lambda(r) = \begin{cases} \Lambda_1, & -\frac{X_1}{2} + nX \le r \le \frac{X_1}{2} + nX \\ \Lambda_2, & \frac{X_1}{2} + nX \le r \le \frac{X_1}{2} + \frac{X_2}{2} + nX \end{cases} \quad (8)$$

where X_1 and X_2 are the two periods of the matter profile or potential, $X = X_1 + X_2$, and n is integer. The parametric resonance condition derived by E. Akhmedov [7] is,

$$\frac{\tan(\omega_{\rm m1} X_1/2)}{\tan(\omega_{\rm m2} X_2/2)} = -\frac{\cos 2\theta_{\rm m2}}{\cos 2\theta_{\rm m1}}, \quad (9)$$

where $\omega_{{\rm m}i}$ and $\theta_{{\rm m}i}$ are the energy difference and mixing angle for potential Λ_1 and Λ_2 respectively.

Even though this castle wall problem is exactly solved, the condition itself is not transparent. In this subsection, we show that such a system is closed related to Rabi oscillations by making appropriate approximation, which will be be specifically proved in Sec. IV.

For illustration purpose, we set the profile to be equal period for the two densities so that $X_1 = X_2 \equiv X/2$. To show that the neutrino flavor conversions in this castle wall matter profiles is related to Rabi oscillation, we decompose the profile using Fourier series,

$$\lambda(r) = \lambda_0 + \sum_{n=1}^{\infty} \lambda_n \cos(k_n r), \quad (10)$$

where

$$\begin{aligned} \lambda_0 &= (\Lambda_1 + \Lambda_2)/2, \\ \lambda_n &= \frac{2}{(2n-1)\pi}(-1)^n (\Lambda_1 - \Lambda_2), \\ k_n &= (2n-1)k_0, \\ k_0 &= 2\pi/X. \end{aligned}$$

To calculate the transitions between two mass states of background matter potential λ_0, we use the background matter basis with respect to λ_0, in which the transition is zero when varying matter profile vanishes. The Hamiltonian

$$H^{(\rm m)} = -\frac{1}{2}\omega_{\rm m}\sigma_3 + \frac{1}{2}\sum_{n=1}^{\infty} \lambda_n \cos 2\theta_{\rm m} \cos(k_n r)\,\sigma_3 - \frac{1}{2}\sum_{n=1}^{\infty} \lambda_n \sin 2\theta_{\rm m} \cos(k_n r)\,\sigma_1, \quad (11)$$

determines the transitions between the two background matter states.

In principle, the base frequency k_0 which is determined by the total period X can be arbitrary. In this example, we choose a X so that the base frequency k_0 matches the energy gap $\omega_{\rm m}$. Even though multiple perturbation frequencies show up in Eq. (11), we identify that only the first frequency $n = 1$ is the resonance frequency since we are using $k_0 = \omega_{\rm m}$. As an approximation, we drop all other frequencies $n > 1$ regarding the fact that they are off-resonance. Thus, similar to single frequency matter profile, the varying σ_3 terms have limited effects on the transition probabilities in our case, which leads to

$$\begin{aligned} H^{(\rm m)} &\to -\frac{1}{2}\omega_{\rm m}\sigma_3 - \frac{1}{2}\lambda_1 \sin 2\theta_{\rm m} \cos(k_0 r)\,\sigma_1 \\ &\to -\frac{1}{2}\omega_{\rm m}\sigma_3 - \frac{1}{2}A_1 \cos(k_0 r)\sigma_1 + \frac{1}{2}A_1 \sin(k_0 r)\sigma_2, \end{aligned}$$

where

$$A_1 = \frac{\lambda_1 \sin 2\theta_{\rm m}}{2}.$$

FIG. 3 shows the neutrino transition probabilities between the two matter states for different $\Lambda_2 - \Lambda_1$. For small $\Lambda_2 - \Lambda_1$, the Rabi formula prediction using the resonance frequency $k_0 = \omega_{\rm m}$ matches the numerical results.

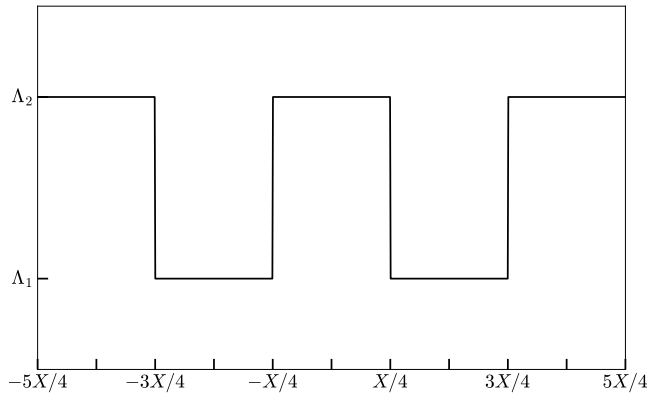

FIG. 2: The castle wall matter potential profile with $X_1 = X_2 = X/2$.

The reason is that the resonance widths of each other frequencies are small compared to the detuning $k_n - \omega_{\rm m}$, so that the interference between the resonance mode and all other modes are small. We notice larger deficit between Rabi formula predictions and numerical results for large $\Lambda_2 - \Lambda_1$, which is due to the destruction effect of the interference with between modes. We will provide a semi-quantitative analysis in the next subsection.

C. Interference Between Different Frequencies

The interference effect between different modes in multiple-frequency Rabi oscillations can be illustrated using a two-mode model. In Fig. 3, the transition amplitude drops for larger fluctuations $\Lambda_2 - \Lambda_1$. Such destruction effect can be interpreted as shift of energy gap due to the long wavelength perturbation. To model the effect, we construct a Rabi oscillation Hamiltonian with two modes of different frequency,

$$H^{(\rm m)} = -\frac{\omega_{\rm m}}{2}\sigma_3 - \frac{1}{2}\sum_{n=1}^{2} A_n \cos(k_n r)\sigma_1 + \frac{1}{2}\sum_{n=1}^{2} A_n \sin(k_n r)\sigma_2. \tag{12}$$

To show the destruction effect, the Hamiltonian Eq. (12) is written as vectors with sigma matrices as the basis,

$$\mathbf{H} = \begin{pmatrix} 0 \\ 0 \\ \omega_m \end{pmatrix} + \begin{pmatrix} A_1\cos(k_1 r) \\ -A_1\sin(k_1 r) \\ 0 \end{pmatrix} + \begin{pmatrix} A_2\cos(k_2 r) \\ -A_2\sin(k_2 r) \\ 0 \end{pmatrix}. \tag{13}$$

The three terms are defined as $\mathbf{H}_3$, $\mathbf{H}_1$, and $\mathbf{H}_2$, where $\mathbf{H}_3$ is perpendicular to the other two vectors. Assuming $\mathbf{H}_2$ is the slow rotating field, i.e., $k_2 < k_1$, the shift of energy gap is calculated as

$$\omega'_{\rm m} = \sqrt{\omega_{\rm m}^2 + A_2^2} \tag{14}$$

$$\approx \omega_{\rm m} + \frac{A_2^2}{2\omega_m}, \tag{15}$$

where we keep only first order of Taylor series.

To begin with, we choose the first rotating perturbation to satisfy the resonance condition $k_1 = \omega_{\rm m}$, the condition for the second slow rotating field shifting the system out of resonance is that the detuning becomes larger than the resonance width,

$$|\omega'_{\rm m} - \omega_{\rm m}| \geq |A_1|, \tag{16}$$

which leads to

$$|A_2| \geq \sqrt{2\omega_{\rm m}|A_1|} \equiv A_{2,\rm Critical}. \tag{17}$$

The relative detuning Q for the resonance frequency also changes from 0 to

$$Q'_1 = \frac{|k_1 - \omega_{\rm m}|}{|A_1|} = \frac{A_2^2}{2\omega_{\rm m}|A_1|}. \tag{18}$$

If the conjecture is correct, we expect the transition amplitude to decrease as we have larger $|A_2|$.

We choose a system with two frequencies where the first frequency has amplitude $A_1 = 10^{-4}\omega_{\rm m}$ and frequency $k_1 = \omega_{\rm m}$. With a small amplitude of the second frequency, $A_2 = 4.5 \times 10^{-4}\omega_{\rm m}$, we obtain almost full resonance. For larger A_2 the destruction effect is more effective, as shown in Fig. 4. The agreement between markers and corresponding lines verifies the approximation that the slow rotating field works as a shift in energy gaps. The relative detunings are 0.001, 1, and 3 for $A_2 = 2.4 \times 10^{-4}\omega_{\rm m}$, $A_2 = A_{2,\rm Critical} = 1.4 \times 10^{-2}\omega_{\rm m}$, and $A_2 = 2.4 \times 10^{-2}\omega_{\rm m}$ respectively. We also notice that the width of each cases doesn't change since we kept A_1 fixed for each calculation, which indicates that the decreasing in transition amplitude is because of the increasing in detuning.

The resonance destruction effect in Fig. 3 is qualitatively described the comparison of relative detunings of different frequencies. The salient feature of this Fourier series expanded matter profile Eq. (10) is that the width of each frequency decreases as the order n increases while the detuning of each frequency increases. We calculate

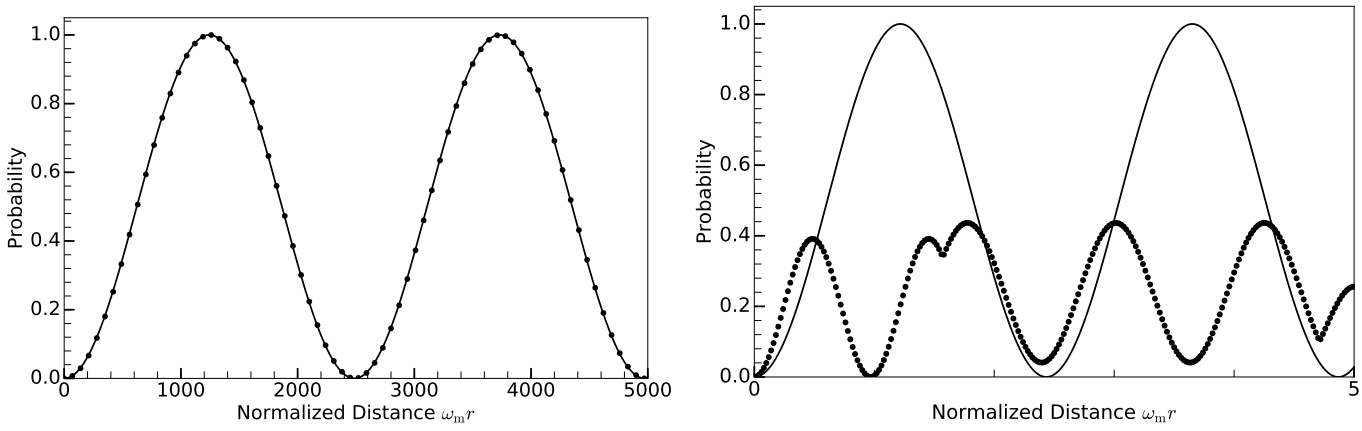

(a) (b)

FIG. 3: Transition probabilities for castle wall matter profile. The black dots, and blue triangles are the transition probabilities of castle wall matter profile calculated numerically for $\Lambda_2 - \Lambda_1 = 0.003\pi\Lambda_0$, and $\Lambda_2 - \Lambda_1 = 3.065\pi\Lambda_0$ respectively, while the black solid line, and blue dashed line are the corresponding Rabi formula. During the calculation, the energy of neutrinos is 10 MeV, mass-squared difference is $\delta m^2 = 2.6 \times 10^{-3}\,\mathrm{eV}^2$, and the vacuum mixing angle chosen so that $\sin^2(2\theta_v) = 0.093$. The background potential Λ_0 is chosen so that it's half the MSW resonance potential, $\Lambda_0 = \frac{1}{2}\lambda_{\mathrm{MSW}} = \frac{1}{2}\omega_{\mathrm{v}} \cos 2\theta_{\mathrm{v}}$, and the base frequency is set to $k_0 = 2\pi/X = \omega_{\mathrm{m}}$.

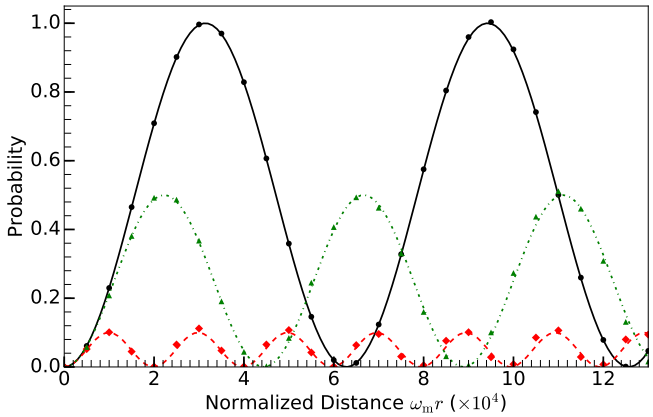

FIG. 4: Reduction of transition amplitudes. Black dots are the numerical transition amplitudes for $A_2 = 4.5 \times 10^{-4}\omega_{\mathrm{m}}$; Green up-pointing triangles are the numerical transition amplitude for $A_2 = A_{2,\mathrm{Critical}} = 1.4 \times 10^{-2}\omega_{\mathrm{m}}$; Red diamonds are the numerical transition amplitudes for $A_2 = 2.4 \times 10^{-2}\omega_{\mathrm{m}}$. In all the calculations, we choose $A_1 = 10^{-4}\omega_{\mathrm{m}}$, $k_1 = \omega_{\mathrm{m}}$, $k_2 = 0.01\omega_{\mathrm{m}}$. The lines are the probabilities predicted using Rabi formula correspondingly. During the calculation, Λ_0 is set to half of the MSW resonance potential, $\Lambda_0 = \frac{1}{2}\lambda_{\mathrm{MSW}} = \frac{1}{2}\omega_{\mathrm{v}} \cos 2\theta_{\mathrm{v}}$.

the relative detuning for each frequency

$$Q_n = \frac{|k_n - \omega_{\mathrm{m}}|}{|\lambda_n \sin 2\theta_{\mathrm{m}}/2|} = \frac{2(n-1)(2n-1)\pi\omega_{\mathrm{m}}}{(\Lambda_2 - \Lambda_1)\sin 2\theta_{\mathrm{m}}} \tag{19}$$

which is quadratic in n. Table I lists the relative detuning for each frequency in Fig. 3a and Fig. 3b. Since the

TABLE I: Relative detuning of each frequency.

	$\Lambda_2 - \Lambda_1 = 0.003\pi\Lambda_0$	$\Lambda_2 - \Lambda_1 = 3.065\pi\Lambda_0$
Q_1	0	0
Q_2	6.1×10^3	6.0
Q_3	2.0×10^4	2.0×10^1
Q_4	4.3×10^4	4.2×10^1

higher order relative detunings Q_n for $n \geq 2$ are much larger than 1 for $\Lambda_2 - \Lambda_1 = 0.003\pi\Lambda_0$, we expect the term with frequency k_1 dominates. In the other situations, the Q_2 term is small which indicates a possible interference between k_2 and k_1 frequency. We perform the approximation Eq. (18) for the Fourier series expanded castle profile and include only the first two frequencies since higher frequencies terms have very large Q's. We find the relative detuning Q_1 change from 0 to 0.001 and 1 for $\Lambda_2 - \Lambda_1 = 0.003\pi\Lambda_0$ and $\Lambda_2 - \Lambda_1 = 3.065\pi\Lambda_0$ respectively. A very small relative detuning $Q_1' = 0.001$ have almost no effect on the transition amplitude which is what we observe in Fig. 3a, while $Q_1' = 1$ will supress the amplitude by half, which mathches what is shown in Fig. 3b.

Fig. 5 shows an intriguing phenomenon we observe. The transition probabilities are for the Hamiltonian of three-frequency matter profile

$$H^{(\mathrm{m})} = -\frac{\omega_\mathrm{m}}{2}\sigma_3 + \frac{1}{2}\sum_{n=1}^{3}\cos 2\theta_\mathrm{m} A_n \sin(k_n r)\sigma_3 - \frac{1}{2}\sum_{n=1}^{3}\sin 2\theta_\mathrm{m} A_n \cos(k_n r)\sigma_1 \tag{20}$$

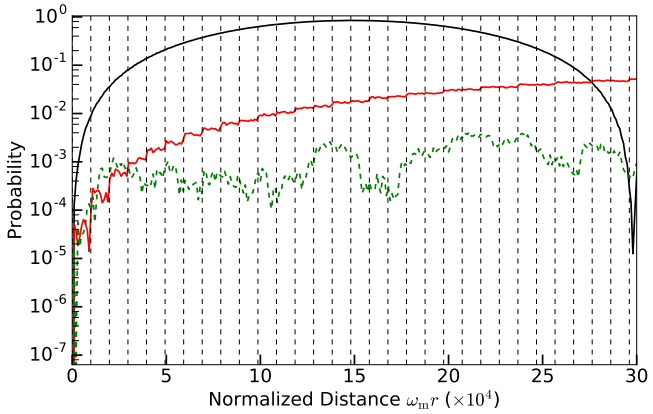

FIG. 5: Resonance destruction due to energy gap shift. The black line is the transition probability for two frequencies $k_1 = \omega_\mathrm{m}$, $k_2 = \omega_\mathrm{m}/\pi$, $A_1 = 10^{-4}\omega_\mathrm{m}$, $A_2 = 1.4\times 10^{-2}\omega_\mathrm{m}$; The red line is the transition probability for two frequencies $k_1 = \omega_\mathrm{m}$, $k_2 = \omega_\mathrm{m}/1000\pi$, $A_1 = 10^{-4}\omega_\mathrm{m}$, $A_2 = 1.4\times 10^{-2}\omega_\mathrm{m}$; The green line is the transition probability for three frequencies $k_1 = \omega_\mathrm{m}$, $k_2 = 1/1000\pi$, $k_3 = \omega_\mathrm{m}/543\pi$, $A_1 = 10^{-4}\omega_\mathrm{m}$, $A_2 = A_3 = 1.4\times 10^{-2}\omega_\mathrm{m}$. The vertical gridlines are the points where the second matter potential becomes 0.

with different combinations of A_n and k_n. The most significant difference from the example for two-frequency interference Eq. (12) is that we have varying energy gap shift. The red line shows the step-like increase in transition probability. Each step-like jump is the point where the second frequency matter potential becomes zero so that the resonance is restored. However, by adding another frequency we have eliminated such resonance restored points since the matter potential of the combination of second and third frequency have no zero points within this range of calculation. This is another verification of our conjecture that the destruction of resonance is due to the energy gap shift, or equivalently the relative detuning. The reason we do not observe this phenomenon in Fig. 3 is because the amplitude of matter potential is decreasing rapidly for for larger n's which leads to a dramatic decrease in relative detuning.

IV. PARAMETRIC RESONANCE AND RABI OSCILLATION — JACOBI-ANGER EXPANSION

With the intuition of the Rabi oscillation itself as well as the interference with long wave length mode shown in Sec. III, we can interpret the transition probabilities of any matter profile more precisely if the system can be exactly decomposed into multiple Rabi oscillations. In this section, we show that the matter effect can be decomposed into superpositions of Rabi oscillations by applying a Jacobi-Anger expansion to the Hamiltonian. Similar trick has been used in Ref. 15. However, we take a different approach by applying a unitary transformation first which make the motivation of Jacobi-Anger expansion, then write the final result as superpositions of Rabi oscillation. For a system with general matter perturbation, c.f. Eq. (4), we apply an unitary transformation of the form

$$\mathbf{U} = \begin{pmatrix} e^{-i\eta(r)} & 0 \\ 0 & e^{i\eta(r)} \end{pmatrix}, \tag{21}$$

which is a transformation used in Ref. 19 to remove the diagonal elements of the Hamiltonian. In this work, this transformation is used to remove the varying σ_3 terms $\delta\lambda(r)\cos 2\theta_\mathrm{m}\sigma_3/2$ in the Hamiltonian, so that the energy gap is fixed in the new basis $(|\nu_{\mathrm{r}1}\rangle, |\nu_{\mathrm{r}2}\rangle)^{\mathrm{T}}$, which is defined as

$$\begin{pmatrix} |\nu_{\mathrm{r}1}\rangle \\ |\nu_{\mathrm{r}2}\rangle \end{pmatrix} = \mathbf{U}^\dagger \begin{pmatrix} |\nu_\mathrm{L}\rangle \\ |\nu_\mathrm{H}\rangle \end{pmatrix}. \tag{22}$$

For convenience, we name this unitary transformation Rabi transformation in Eq. (21) as well as the new basis in Eq. (22) the Rabi basis. In Rabi basis, we find the Schrödinger equation

$$\begin{pmatrix} \frac{\mathrm{d}\eta}{\mathrm{d}r} & 0 \\ 0 & -\frac{\mathrm{d}\eta}{\mathrm{d}r} \end{pmatrix}\begin{pmatrix}\psi_{\mathrm{R}1}\\ \psi_{\mathrm{R}2}\end{pmatrix} + \mathrm{i}\frac{\mathrm{d}}{\mathrm{d}r}\begin{pmatrix}\psi_{\mathrm{R}1}\\ \psi_{\mathrm{R}2}\end{pmatrix} = \left[-\frac{\omega_\mathrm{m}}{2}\sigma_3 + \frac{\delta\lambda}{2}\cos 2\theta_\mathrm{m}\sigma_3 - \frac{\delta\lambda}{2}\sin 2\theta_\mathrm{m}\begin{pmatrix} 0 & e^{2\mathrm{i}\eta} \\ e^{-2\mathrm{i}\eta} & 0\end{pmatrix}\right]\begin{pmatrix}\psi_{\mathrm{R}1}\\ \psi_{\mathrm{R}2}\end{pmatrix},$$

in which the varying diagonal elements in Hamiltonian can be eliminated by choosing $\eta(x)$ properly, i.e.,

$$\eta(x) - \eta(0) = \frac{\cos 2\theta_\mathrm{m}}{2}\int_0^x \delta\lambda(\tau)d\tau. \tag{23}$$

In Rabi basis, the Schrödinger equation becomes

$$i\frac{d}{dx}\begin{pmatrix}\psi_{\mathrm{r}1}\\ \psi_{\mathrm{r}2}\end{pmatrix} = \left[-\frac{\omega_\mathrm{m}}{2}\sigma_3 - \frac{\delta\lambda}{2}\sin 2\theta_m\begin{pmatrix} 0 & e^{2i\eta} \\ e^{-2i\eta} & 0\end{pmatrix}\right]\begin{pmatrix}\psi_{\mathrm{r}1}\\ \psi_{\mathrm{r}2}\end{pmatrix},$$

where $\eta(x) = -A_1 \cos 2\theta_{\rm m} \cos(k_1 x)/(2k)$ for single frequency matter profile with potential $\delta\lambda(x) = A_1 \sin(k_1 x)$. One can easily show that the transition probability between two eigenstates in Rabi basis is the same as the transition probability between two eigenstates in background matter basis.

To make connection with Rabi oscillation, we apply Jacobi-Anger expansion, which is used in Ref. 15, to decompose the $\exp(iz\cos(k_1 r))$-like term in Hamiltonian into linear combinations of terms that is proportional to $\exp(ink_1 r)$, i.e., to decompose spherical waves into plane waves. The decomposed form of Hamiltonian explicitly shows that the Hamiltonian is a summation of Rabi systems, which is

$$H^{(\rm R)} = -\frac{\omega_{\rm m}}{2} - \frac{1}{2}\sum_{n=-\infty}^{\infty} B_n \begin{pmatrix} 0 & \Phi_n e^{ink_1 r} \\ \Phi_n^* e^{-ink_1 r} & 0 \end{pmatrix},$$

where

$$B_n = \tan 2\theta_{\rm m} n k_1 J_n\left(\frac{A_1}{k_1}\cos 2\theta_{\rm m}\right),$$
$$\Phi_n = e^{i\pi(3n/2+1)},$$

with J_n standing for the Bessel function. The constant phase Φ_n doesn't play any role for the reason discussed in Appendix A. Phase in matter potential would also go into Φ_n, for which reason, phase is not included in the current problem. The first term in Hamiltonian describes the energy gap, while the second term is the summation of many driving fields. The resonance width for a given mode n is $|B_n|$. It's worth mentioning that for large n, we have [20]

$$J_n(n\,\mathrm{sech}\,\alpha) \sim \frac{e^{n(\tanh\alpha-\alpha)}}{\sqrt{2\pi n \tanh\alpha}}. \tag{24}$$

It's straightforward to prove that resonance width decreases dramatically for large n thus higher order modes become insignificant.

When the system has one dominate resonance mode and without significant interference between the resonance mode and other modes, all off-resonance modes can be dropped without significantly changing the transition probabilities. However, as we have shown previously in Sec. III, interference might happen between different modes. A qualitative measure should be introduced so that we know what the conditions are for dropping other modes. The following subsections will determine the important modes of the system (i.e., which n to include) and explore the interference between modes hence explain the coincidence presented in the previous sections. For numerical calculations, we use dimensionless quantities which are scaled using the characteristic energy scale $\omega_{\rm m}$, e.g.,

$$\hat{r} = \omega_{\rm m} r,$$
$$\hat{k}_1 = \frac{k_1}{\omega_{\rm m}},$$
$$\hat{A}_1 = \frac{A_1}{\omega_{\rm m}},$$
$$\hat{B}_n = \frac{B_n}{\omega_{\rm m}}.$$

Through the Rabi transformation and Jacobi-Anger expansion, the varying diagonal elements in Hamiltonian, i.e., varying σ_3 term, is transformed to a perturbing field with many different frequencies nk_1.

A. The Important Factors

To determine the important modes and justify the approximations used in Sec. III, the resonance width for each mode which is determined by B_n, the deviation from exact resonance (i.e., detuning) which is calculated as $|nk_1 - \omega_{\rm m}|$, and oscillation wavelength of each mode compared to the size of the physical system should be considered.

More specifically, we define the resonance quality of each mode using the reciprocal of scaled detuning

$$Q_n = |B_n/(nk_1 - \omega_{\rm m})|, \tag{25}$$

which measures how well the resonance is. For exact resonance, $Q_n = 0$, while large Q_n says the system is too far away from the resonance of this specific mode. Small Q_n modes are the modes that are dramatically important to the system. Meanwhile, modes that has much larger oscillation wavelength are not subjected to be considered even though their Q_n's are close to zero, which is due to the fact that such modes have not accumulated much transition probabilities within the size of the physical system.

Similar quantities are to be considered for multi-frequency matter profile, such as the resonance width of each mode B_N, detuning $|\sum_a n_a k_a - \omega_{\rm m}|$, and Rabi frequency Ω_N, as well as $Q_N = |B_N/(\sum_a n_a k_a - \omega_{\rm m})|$.

In principle, we can always approximate the system by including more modes with larger relative detuning while neglecting the modes with wavelength much longer than the size of physical system. Notheless such effort doesn't simplify the calculations.

B. Single Frequency Matter Profile

For the single frequency matter potential $\lambda = \lambda_0 + \lambda_1 \sin(k_1 r)$ discussed in Sec. III A, we removed the varying σ_3 term by arguing that this term has no effect on transition probabilities when the system is close to resonance, $k_1 \sim \omega_{\rm m}$. The reason is that only the first mode

$n = 1$ is on resonance when $k_1 = \omega_{\rm m}$ and all other modes are far from resonance, thus

$$H^{\rm R} \approx -\frac{\omega_{\rm m}}{2}\sigma_3 - \frac{1}{2}B_1 \begin{pmatrix} 0 & \Phi_1 e^{ik_1 r} \\ \Phi_1^* e^{-ik_1 r} & 0 \end{pmatrix} \quad (26)$$
$$\approx -\frac{\omega_{\rm m}}{2}\sigma_3 - \frac{A_1}{2}\cos(k_1 r)\sigma_1 + \frac{A_1}{2}\sin(k_1 r)\sigma_2,$$

where A_1 is defined in Eq. (7) and approximation

$$J_1\left(\frac{\lambda_1}{k_1}\cos(2\theta_{\rm m})\right) \approx \frac{\lambda_1}{2k_1}\cos(2\theta_{\rm m})$$

for small $\lambda_1\cos(2\theta_{\rm m})/k_1$ is used in the last step. Thus we reach a similar equation to the approximation we used in Sec. III A. Small $\lambda_1\cos(2\theta_{\rm m})/k_1$ corresponds to small resonance width for Eq. (6) and also Eq. (26) so that the interferences are small. For $\lambda_1\cos(2\theta_{\rm m})/k_1 \gg 1$, the resonance width is very large compared to $|nk_1 - \omega_{\rm m}$, which is the distance between different order of resonances, thus bringing in the interference between different modes. The relative detuning for each mode in the Jacobi-Anger expansion for single frequency matter profile used in Fig. 1 is calculated, which shows that the relative detuning of the first mode is 0, while the relative detuning of the second and third mode are 1.1×10^9 and 9.7×10^{13} which are too huge to have any effect on the overall transition probability.

C. Multifrequency Matter Profile

The interference effect shown in Fig. 5 is also interpretable by means of Jacobi-Anger expansion. Table II shows the smallest relative detunings and corresponding oscillation wavelength of each mode. As expected, the third frequency introduced many small relative detuning modes, which interferes more compared to the two frequency cases.

A matter profile as complicated as the castle wall profile can be decomposed into a summation of multiple frequencies. Even for arbitrary multi-frequency matter potential

$$\lambda(r) = \lambda_0 + \sum_n A_n \sin(nk_n r), \quad (27)$$

the Hamiltonian also takes a form of summation of Rabi oscillations,

$$H^{(\rm R)} = -\frac{\omega_{\rm m}}{2} - \frac{1}{2}\sum_{n_1=-\infty}^{\infty}\cdots\sum_{n_N=-\infty}^{\infty} B_{\{n_i\}} \begin{pmatrix} 0 & \Phi_{\{n_i\}} e^{i(\sum_a n_a k_a)r} \\ \Phi^*_{\{n_i\}} e^{-i(\sum_a n_a k_a)r} & 0 \end{pmatrix}, \quad (28)$$

where

$$B_{\{n_i\}} = \tan 2\theta_{\rm m}\left(\sum_a n_a k_a\right)\left(\prod_a J_{n_a}\left(\frac{A_a}{k_a}\cos 2\theta_m\right)\right),$$
$$\Phi_{\{n_i\}} = e^{i\pi(3\sum_a n_a/2+1)},$$

which is similar to the single frequency matter potential Hamiltonian. A mode is defined by a certain choice of $n_1, \cdots, n_N$. As defined for single frequency matter profile, a relative detuning can also be defined for multi-frequency matter profile

$$Q_{\{n_i\}} = \frac{|\sum_a n_a k_a - \omega_{\rm m}|}{|B_{\{n_i\}}|}. \quad (29)$$

As the number of frequencies becomes large, the resonance modes are easily clogged together since many set of $\{n_i\}$'s can be chosen so that the relative detunings are all close to 0. Resonance modes that has oscillation wavelength much larger than the physical system such as supernova explosion are neglected since these modes have not developed large transition probabilities within the size of the physical system. On the other hand, long wavelength modes are the source of resonance destruction for short wavelength resonance modes, as shown in Sec. III C.

V. CONCLUSIONS

In conclusion, we have provided a novel interpretation for neutrino flavor conversion in matter. The first step was to interpret the neutrino flavor conversions in background matter basis. By intuition, we interpreted the neutrino flavor conversion in a single frequency matter profile as Rabi oscillations when the matter fluctuation frequency is close to the energy gap, which is one of the resonance conditions. We anticipated the matter density fluctuations which introduced a varying part in the energy gap have limited effects on neutrino flavor conversions given the matter fluctuation frequency matches the background energy gap, so that the matter fluctuation only works as a pure flipping field that converts neutrinos from one flavor to another. Relative detuning has been the key to this paper since it is critical to quantify how off-resonance a Rabi oscillation is. In the case of single frequency matter profile, the relative detuning becomes 0 under the resonance condition. We also showed

TABLE II: Relative detuning and oscillation wavelength of each mode.

$k_2 = \omega_{\rm m}/\pi$			$k_2 = \omega_{\rm m}/1000\pi$			three-frequency		
$\{n_i\}$	Q	λ	$\{n_i\}$	Q	λ	$\{n_i\}$	Q	λ
1,0	0.	324472.	1,0	0.	3.32075×10^6	1,0,0	0.	2.29097×10^7
0,1	248.873	9.217	1,1	215.309	19739.	1,35,-19	17.913	2.1229×10^6
0,-1	481.292	4.76608	1,-1	215.446	19739.	1,-35,19	17.9131	2.1231×10^6
0,2	6477.51	17.2909	1,2	323.895	9869.56	1,-11,6	53.225	359495
0,-2	29173.9	3.83912	1,-2	324.307	9869.56	1,11,-6	53.2267	359556
0,3	78458.1	139.408	1,4	590.72	4934.8	1,37,-20	63.8707	241920
-1,0	103283.	3.14159	1,-4	592.226	4934.8	1,-37,20	63.8775	241992.
1,1	608730.	19.7392	1,3	741.798	6579.73	1,-22,12	111.436	162934.
1,-1	1.17721×10^6	19.7392	1,-3	743.216	6579.73	1,22,-12	111.443	163032.

that the interference in Rabi oscillations between a high frequency matter profile, which is on-resonance and a low frequency matter profile, which is off-resonance, is related to the shift in energy gap. Consequently, the strength of interference is measured by modification of relative detuning due to the shift of energy gap.

Neutrino flavor conversions in matter can also be described in a basis where the oscillations are consequences of superposition of Rabi oscillations, which are modes of oscillations. This view was applied to emphasis the approximations that the change of energy gap due to matter fluctuation can be neglected under resonance condition in the previous background matter basis. The destruction effect due to multiple frequencies matter profile was also explained as the interference between different modes. If only one mode has a close to zero relative detuning while all other modes have much larger relative detunings, only the one with small relative detuning dominates the neutrino flavor conversion. Otherwise, interferences serves as a destruction effect of the neutrino flavor conversion.

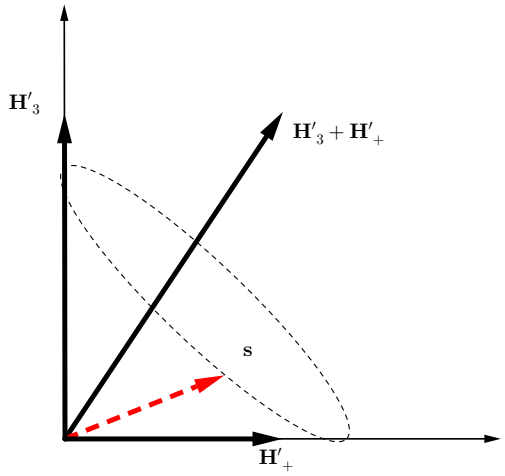

FIG. 6: Rabi oscillations in static frame and rotating frame. In both figures the red dashed vector is the flavor isospin, while the black solid vectors are the vectors of Hamiltonian. The left panel shows the rotating Hamiltonian $\mathbf{H}_3 + \mathbf{H}_+$. The right panel shows the rotation of flavor isospin around a static vector $\mathbf{H}'_3 + \mathbf{H}'_+$ in the rotating frame.

VI. ACKNOWLEDGEMENT

The first author would like to thank J. Kneller and K. Patton for their help during this research.

Appendix A: Rabi Oscillations

In this appendix we introduce flavor isospin [18] to Rabi oscillations and derive the transition probabilities as well as explain the resonance and width briefly.

The Hamiltonian for Rabi oscillation is

$$H_{\rm R} = -\frac{\omega_{\rm R}}{2}\sigma_3 - \frac{A_{\rm R}}{2}\left(\cos(k_{\rm R}t+\phi_{\rm R})\sigma_1 - \sin(k_{\rm R}t+\phi_{\rm R})\sigma_2\right), \tag{A1}$$

in which $\omega_{\rm R}$ serves as the energy split of the two level system, while $A_{\rm R}$ and $k_{\rm R}$ are the strength and frequency of the driving field, respectively. A decomposition of the second term shows that

$$H_{\rm R} = -\frac{\boldsymbol{\sigma}}{2}\cdot(\mathbf{H}_3 + \mathbf{H}_+),$$

where $\boldsymbol{\sigma}$ is the the vector of Pauli matrices, and the three vectors are

$$\mathbf{H}_3 = \begin{pmatrix} 0 \\ 0 \\ \omega_{\rm R} \end{pmatrix}, \tag{A2}$$

$$\mathbf{H}_+ = \begin{pmatrix} A_{\rm R}\cos(k_{\rm R}t+\phi_{\rm R}) \\ -A_{\rm R}\sin(k_{\rm R}t+\phi_{\rm R}) \\ 0 \end{pmatrix}. \tag{A3}$$

The three vectors are mapped onto a Cartesian coordinate system, so that $\mathbf{H}_3$ is the vector aligned with the third axis, $\mathbf{H}_+$ is a rotating vectors in a plane perpendicular to $\mathbf{H}_3$. The wave function $\Psi = (\psi_1, \psi_2)^{\rm T}$ is also

used to define the state vector $\mathbf{s}$

$$\mathbf{s} = \Psi^\dagger \frac{\boldsymbol{\sigma}}{2} \Psi \tag{A4}$$

$$= \frac{1}{2} \begin{pmatrix} 2\,\mathrm{Re}\,(\psi_1^* \psi_2) \\ 2\,\mathrm{Im}\,(\psi_1^* \psi_2) \\ |\psi_1|^2 - |\psi_2|^2 \end{pmatrix} \tag{A5}$$

The third component of $\mathbf{s}$, which is denoted as s_3, is within range $[-1/2, 1/2]$. The two limits, $s_3 = -1/2$ and $s = 1/2$ stand for the system in high energy state and low energy state respectively. $s_3 = 0$ if the system has equal probabilities to be on high energy state and low energy state. The Schrödinger equation becomes

$$\frac{\mathrm{d}}{\mathrm{d}t}\mathbf{s} = \mathbf{s} \times \mathbf{H}, \tag{A6}$$

which is the precession equation. For static $\mathbf{H}$, the state vector $\mathbf{s}$ precess around $\mathbf{H}$.

In a frame that corotates with $\mathbf{H}_+$, which is described in Fig. 6, the new Hamiltonian is

$$\frac{\mathrm{d}}{\mathrm{d}t}\mathbf{s} = \mathbf{s} \times (\mathbf{H}_3' + \mathbf{H}_+), \tag{A7}$$

where

$$\mathbf{H}_3' = \begin{pmatrix} 0 \\ 0 \\ \omega_\mathrm{R} - k_\mathrm{R} \end{pmatrix}, \qquad \mathbf{H}_+' = \begin{pmatrix} A_\mathrm{R} \\ 0 \\ 0 \end{pmatrix}. \tag{A8}$$

The state vector $\mathbf{s}$ precess around a static vector $\mathbf{H}_3' + \mathbf{H}_+'$ with a frequency $\Omega_\mathrm{R} = \sqrt{|A_\mathrm{R}|^2 + (k_\mathrm{R} - \omega_\mathrm{R})^2}$. A geometric analysis by projecting the state vector $\mathbf{s}$ on to the verticle axis shows that

$$s_3 = \frac{1}{2} - \frac{|A_\mathrm{R}|^2}{\Omega_\mathrm{R}^2} \sin^2\left(\frac{\Omega_\mathrm{R}}{2} t\right). \tag{A9}$$

Resonance occurs when the term $\mathbf{H}_3$ disappears in this corotating frame, since the state vector $\mathbf{s}$ converts completely between $+1/2$ (low energy state) and $-1/2$ (high energy state).

Such a system has analytical transition probability from low energy state to high energy state

$$P(r) = \frac{1}{2}(1 - 2s_3(r)) = \frac{|A_\mathrm{R}|^2}{\Omega_\mathrm{R}^2} \sin^2\left(\frac{\Omega_\mathrm{R}}{2} t\right), \tag{A10}$$

where

$$\Omega_\mathrm{R} = \sqrt{|A_\mathrm{R}|^2 + (k_\mathrm{R} - \omega_\mathrm{R})^2} \tag{A11}$$

is known as Rabi frequency. The detuning, which is defined by $k_\mathrm{R} - \omega_\mathrm{R}$, determines how off-resonance the system is, and amplitude of driving field A_R determines the resonance width,

$$\text{Detuning} = |k_\mathrm{R} - \omega_\mathrm{R}|, \tag{A12}$$

$$\text{Resonance Width} = |A_\mathrm{R}|. \tag{A13}$$

The transition probability oscillates with frequency Ω_R. However, the amplitude A_1 is the dominate factor for oscillation frequency when the system is close to resonance. The phase of the matter potential ϕ_R has no effect on the transition probability since it only determines the initial phase of driving Hamiltonian vector $\mathbf{H}_+$. We also notice that the transition amplitude is determined by relative detuning Q, which is defined as

$$Q = \left| \frac{k_\mathrm{R} - \omega_\mathrm{R}}{A_\mathrm{R}} \right|. \tag{A14}$$

Given a Rabi oscillation system with two driving frequencies

$$H_\mathrm{R} = -\frac{\omega_\mathrm{R}}{2}\sigma_3 - \frac{A_1}{2}\left(\cos(k_1 t + \phi_1)\sigma_1 - \sin(k_1 t + \phi_1)\sigma_2\right) - \frac{A_2}{2}\left(\cos(k_2 t + \phi_2)\sigma_1 - \sin(k_2 t + \phi_2)\sigma_2\right)$$

we decompose it into $\mathbf{H}_\mathrm{R} = \mathbf{H}_3 + \mathbf{H}_1 + \mathbf{H}_2$, where

$$\mathbf{H}_1 = \begin{pmatrix} A_1 \cos(k_1 t + \phi_1) \\ A_1 \sin(k_1 t + \phi_1) \\ 0 \end{pmatrix}, \mathbf{H}_2 = \begin{pmatrix} A_2 \cos(k_2 t + \phi_2) \\ A_2 \sin(k_2 t + \phi_2) \\ 0 \end{pmatrix}.$$

Assume $\mathbf{H}_1$ is the on-resonance perturbation which requires $k_1 = \omega_\mathrm{R}$. The most general condition that we can drop the new perturbation $\mathbf{H}_2$ is to make sure k_2 is far from the resonance condition compared to the resonance width,

$$Q \equiv \frac{|k_2 - \omega_\mathrm{R}|}{|A_2|} \gg 1. \tag{A15}$$

A more applicable condition is derived in Sec. III C.

[1] S. P. Mikheev and A. Yu. Smirnov, Sov. J. Nucl. Phys. **42**, 913 (1985), [Yad. Fiz.42,1441(1985)].

[2] L. Wolfenstein, Physical Review D **17**, 2369 (1978).

[3] L. Wolfenstein, Physical Review D **20**, 2634 (1979).

[4] S. Petcov and M. Piai, Physics Letters B **533**, 94 (2002), arXiv:hep-ph/0112074 [hep-ph].

[5] T. K. Kuo and J. Pantaleone, Reviews of Modern Physics **61**, 937 (1989).

[6] P. Krastev and A. Smirnov, Physics Letters B **226**, 341 (1989).

[7] E. K. Akhmedov, Pramana **54**, 47 (2000), arXiv:9907435 [hep-ph].

[8] E. Akhmedov, Nuclear Physics B **538**, 25 (1999), arXiv:hep-ph/9805272 [hep-ph].

[9] S. T. Petcov, Physics Letters B **434**, 321 (1998), arXiv:9805262 [hep-ph].

[10] B. Muller and H.-T. Janka, Monthly Notices of the Royal Astronomical Society **448**, 2141 (2015).

[11] S. M. Couch and C. D. Ott, The Astrophysical Journal **799**, 5 (2015).

[12] F. N. Loreti and A. B. Balantekin, Physical Review D **50**, 4762 (1994), arXiv:9406003 [nucl-th].

[13] A. Friedland and A. Gruzinov, "Neutrino signatures of supernova turbulence," (2006), arXiv:0607244 [astro-ph].

[14] J. Kneller and C. Volpe, Physical Review D **82**, 123004 (2010), arXiv:1006.0913.

[15] J. P. Kneller, G. C. McLaughlin, and K. M. Patton, Journal of Physics G: Nuclear and Particle Physics **40**, 055002 (2013), arXiv:arXiv:1202.0776v1.

[16] K. M. Patton, J. P. Kneller, and G. C. McLaughlin, Physical Review D **89**, 073022 (2014), arXiv:arXiv:1407.7835v1.

[17] R. W. Boyd, *Nonlinear Optics*, 3rd ed. (Elsevier, 2008).

[18] H. Duan, G. M. Fuller, and Y.-Z. Qian, Physical Review D **74**, 123004 (2006), arXiv:0703776 [astro-ph].

[19] J. P. Kneller and G. C. McLaughlin, Physical Review D **73**, 056003 (2006).

[20] I. Ploumistakis, S. Moustaizis, and I. Tsohantjis, Physics Letters A **373**, 2897 (2009).